Journal of ELECTRONIC MATERIALS, Vol. 46, No. 12, 2017
DOI: 10.1007/s11664-017-5744-x


# Plasmon-Assisted Efficiency Enhancement of $Eu^{3+}$-Doped Tellurite Glass-Covered Solar Cells

BISMARCK C. LIMA,[1] L.A. GÓMEZ-MALAGÓN ,[2,5] A.S.L. GOMES,[1] J.A.M. GARCIA,[3] and L.R.P. KASSAB[4]

1.—Department of Physics, Federal University of Pernambuco, Recife, PE 50670-901, Brazil. 2.—Polytechnic School of Pernambuco, University of Pernambuco, Recife, PE 50720-001, Brazil. 3.—Polytechnic School of University of São Paulo, São Paulo, SP 05508-010, Brazil. 4.—Faculty of Technology of São Paulo, CEETEPS/UNESP, São Paulo, SP 01124-060, Brazil. 5.—e-mail: lagomezma@poli.br

Rare-earth-doped tellurite glass containing metallic nanoparticles can be exploited to manage the solar spectrum in order to increase solar cell efficiency. It is therefore possible to modify the incident solar spectrum profile to the spectrum that optimizes the solar cell recombination process by covering the solar cell with plasmonic luminescent downshifting layers. With this approach, the losses due to thermalization are minimized and the efficiency is increased. Due to the down-conversion process that couples the plasmon resonance of the metallic nanoparticles and the rare-earth electronic energy levels, it is possible to convert photons from the ultraviolet region to the visible and near-band-gap region of the semiconductor. It is demonstrated here that plasmon-assisted efficiency enhancements of 14.0% and 34.5% can be obtained for commercial Si and GaP solar cells, respectively, covered with $Eu^{3+}$-doped $TeO_2$-ZnO glass containing silver nanoparticles.

**Key words:** Photovoltaic cells, solar cell, down-conversion, tellurite glass

## INTRODUCTION

One of the goals of photovoltaic (PV) devices is to maximize the conversion of solar energy in electricity. To quantify this relationship and to compare different devices and technologies, measurements of the efficiency are carried out for each photovoltaic technology. In the search to increase the efficiency of solar cells, new materials for the PV cell and techniques to modify the solar spectrum have been continuously researched. State of the art materials and technologies are reported annually by the National Renewable Energy Laboratory (NREL) and by the Solar Efficiency Tables, which show how the efficiency of different technologies has been varying with time.[1,2] In these reports, the efficiency measurements are performed using the standard solar spectrum. However, the mismatch between the solar spectrum and the band gap of photovoltaic materials can decrease the efficiency. Photons with energy below the band gap are not absorbed, and photons with energy higher than the band gap can be absorbed to produce the photovoltaic effect or to introduce losses due to the thermalization process. To avoid or mitigate this effect, down-conversion and up-conversion processes in rare-earth ion-doped glass have been proposed as an alternative approach to this problem.[3] It is worth mentioning that alternative designs have been proposed to enhance the efficiency of silicon solar cells. For example, crystalline silicon solar cells covered with $SiO_2$ can enhance the efficiency up to 14.98% compared to the bare cell. This enhancement can be boosted to 18.7% if it is also covered with a layer of 3 wt.% Eu-doped phosphor particles. The efficiency enhancement was attributed to the broadband reduction in reflectance due to destructive interference of the reflected light between the air/$SiO_2$ and $SiO_2$/Si interfaces and also to the absorption of incident light by Eu-doped phosphor

(Received November 14, 2016; accepted August 8, 2017; published online August 18, 2017)

particles.[4] As another example, for dye-sensitized solar cells (DSSC), a novel design demonstrated that introducing the rare-earth compound europium ion-doped yttrium fluoride ($YF_3$:5%$Eu^{3+}$) in $TiO_2$ film enables the enhancement of its efficiency up to 32% when compared to the DSSC without $YF_3$:$Eu^{3+}$ doping. This enhancement was due to the down-conversion luminescence of $Eu^{3+}$ from ultraviolet light to visible light, and also to the changes in the $TiO_2$ energy level improving the carrier transport at the interface of $TiO_2$/dye.[5]

Down-conversion and up-conversion processes can be enhanced when the local field near the luminescent ions is increased through the surface plasmon resonance (SPR) present at the nanoparticles dielectric-metallic interface. Several publications have reported the spectroscopic characterization of rare-earth-doped glass for photovoltaic applications and also how the luminescence is increased using metallic nanostructures.[6–8] However, a relatively small number of papers have reported the efficiency behavior of solar cells under the modified spectrum.[9–13] On the other hand, the SPR has also been explored to improve the efficiency of thin-film solar cells by increasing the light absorption through the light-scattering and near-field concentration of light when metallic nanoparticles are incorporated into or on the solar cell.[14] These works show that the SPR is an interesting mechanism to improve solar cell efficiency.

The present work reports the efficiency enhancement of silicon and gallium phosphide solar cells covered with tellurite glass ($TeO_2$-ZnO) doped with $Eu^{3+}$ containing silver nanoparticles, in order to exploit the SPR enhancement effect.

## EXPERIMENTAL

Samples of tellurite glass were prepared using the melting quenching technique,[15] with the starting composition (in wt.%) of 85.0 $TeO_2$-15.0 ZnO. The glass samples were prepared with 1 wt.% of $Eu_2O_3$ and also with 2 wt.% of $AgNO_3$. An un-doped sample (without $Eu_2O_3$ and $AgNO_3$) was prepared to be used as reference. Reagents were melted at 835°C in a platinum crucible for 1 h, quenched in a pre-heated brass mold, annealed at 325°C for 2 h, and cooled to room temperature in the furnace to avoid internal stress. Samples with approximately 10 mm length, 4 mm width and 3 mm thickness were cut and polished. A 200-kV high-transmission electron microscope (TEM) was used to investigate the nucleation of the silver nanoparticles, their shape and size. Electron diffraction measurements were performed to determine the crystalline nature of the silver nanoparticles in the tellurite glass.

The optical absorption spectra were obtained using a CARY 5000 Ultraviolet–Visible-Infrared (UV–VIS–IR) spectrophotometer in the range of 300–800 nm. The emission spectra were measured using an Ocean Optics spectrometer and cw lasers operating at 405 nm and 473 nm. Electrical characterization was carried out using a solar simulator (LCS-100 Newport), with a AM 1.5 filter and a sourcemeter (Keithley 2420) coupled to a personal computer. Efficiency, fill factor (*FF*), short circuit current, $I_{sc}$, and open circuit voltage, $V_{oc}$, were obtained from the current–voltage (*I–V*) curves obtained under 1000-W/$m^2$ irradiance of commercial silicon (BPW34 Vishay Semiconductors) and GaP (FGAP71 Thorlabs) semiconductor photodiodes, with energy gaps of 1.1 eV and 2.26 eV, respectively. We note that, during the electrical characterization, the glass samples were placed on top of the solar cell without any glue or attachment.

## RESULTS AND DISCUSSIONS

Figure 1 presents the TEM image and the electron diffraction pattern of a small region of a $TeO_2$-ZnO glass doped with 1 wt.% of $Eu_2O_3$ and 2 wt.% of $AgNO_3$; a spherical silver (Ag) nanoparticle with a polycrystalline structure (inset in Fig. 1) and average diameter around 25 nm can be clearly seen.

Absorption and emission spectra are shown in Figs. 2 and 3. Figure 2 presents the absorption spectra of the samples doped with $Eu^{3+}$ ions, with and without Ag nanoparticles; the absorption transitions associated with the $Eu^{3+}$ ions correspond to the bands centered at 395 nm ($^7F_0 \rightarrow {}^5L_6$), 466 nm ($^7F_0 \rightarrow {}^5D_2$) and 537 nm ($^7F_1 \rightarrow {}^5D_1$).[16] Also, the bandgap of the $TeO_2$-ZnO glass around 380 nm is observed. We estimate the SPR wavelength at between 450 and 500 nm, considering the refractive index (~2) and the dielectric function of silver.[17] However, due to the low concentration of nanoparticles, the typical SPR resonance is not observed in the absorption spectra. There is a lack of a

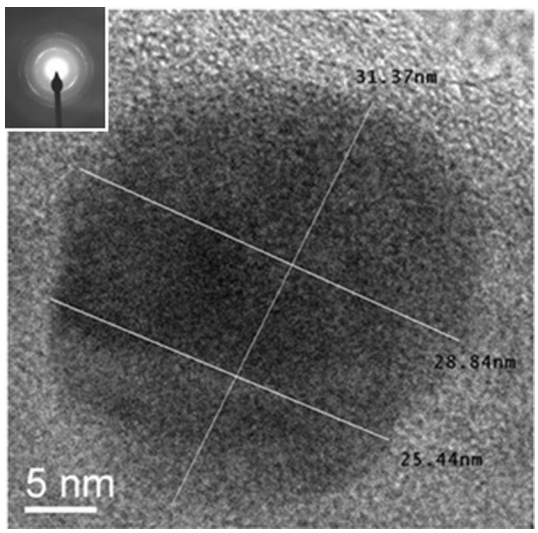


Fig. 1. TEM image of the silver nanoparticle in $TeO_2$-ZnO glass doped with 1 wt.% of $Eu_2O_3$ and 2 wt.% of $AgNO_3$. The average size of 25 nm was determined for the silver nanoparticles. Inset the electron diffraction pattern.

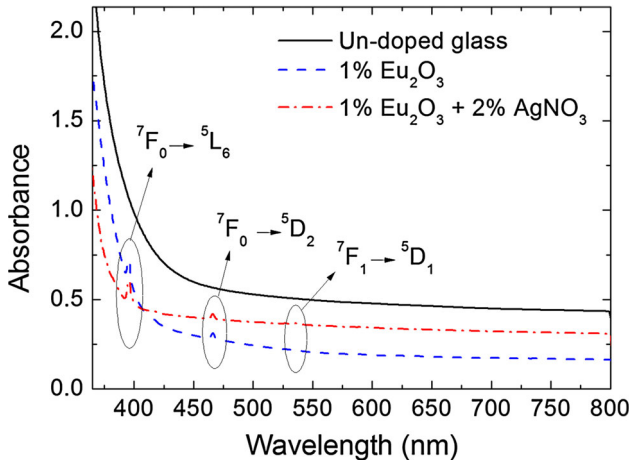


Fig. 2. Absorption spectra of $Eu^{3+}$-doped $TeO_2$-ZnO glass samples with and without Ag nanoparticles; the un-doped glass is shown as reference.

noticeable signal due to the overlap of the weak SPR absorption band and the absorption bands of $Eu^{3+}$ ions, also affected by the fact that the glass matrix absorbs in the blue region.[18,19] Similar tellurite glass samples doped with Ag nanoparticles showed the SPR around 500 nm.[20] Figure 3a and b presents the emission spectra of the samples excited at 405 nm and 473 nm, respectively. The emission bands centered at 510 nm, 536 nm, 556 nm, 580 nm, 593 nm, 613 nm, 655 nm, and 701 nm are attributed to the $Eu^{3+}$ $^5D_2 \rightarrow {}^7F_3$, $^5D_1 \rightarrow {}^7F_1$, $^5D_1 \rightarrow {}^7F_2$, $^5D_0 \rightarrow {}^7F_J$ (with $J = 0, 1, 2, 3$, and 4) transitions, respectively, as shown in the simplified energy levels of $Eu^{3+}$ ion in Fig. 4. The shaded area in Fig. 4 indicates the location of the silver surface plasmon resonance.[16,21] We observe that, at a low concentration of the $Eu_2O_3$ (1 wt.%), the luminescence in the visible spectrum is increased in the presence of Ag nanoparticles. For excitation at 473 nm, Fig. 3b, the emissions around 510 nm, 536 nm, 556 nm, 580 nm and 613 nm were enhanced by almost 100%. However, for excitation at 405 nm (Fig. 3a) the enhancement is lower. The luminescence enhancement depends on the relative distance between the ions and the nanoparticles, the SPR band position, the excitation and emission wavelengths, and the dielectric constants of the nanoparticles and host environment.[22] The proximity of the excitation wavelength to the SPR wavelength plays an important role in the luminescence enhancement as it increases both excitation and emission rates. The larger influence of the nanoparticles on the luminescence of rare-earth ions is observed when the incident light and/or the luminescence frequency are close to the resonance frequency of the surface plasmon.[19] So, the highest enhancement observed for excitation at 473 nm indicates that it is closer to the SPR wavelength than the excitation at 405 nm. For excitation at 473 nm, the increase is attributed to the enhanced

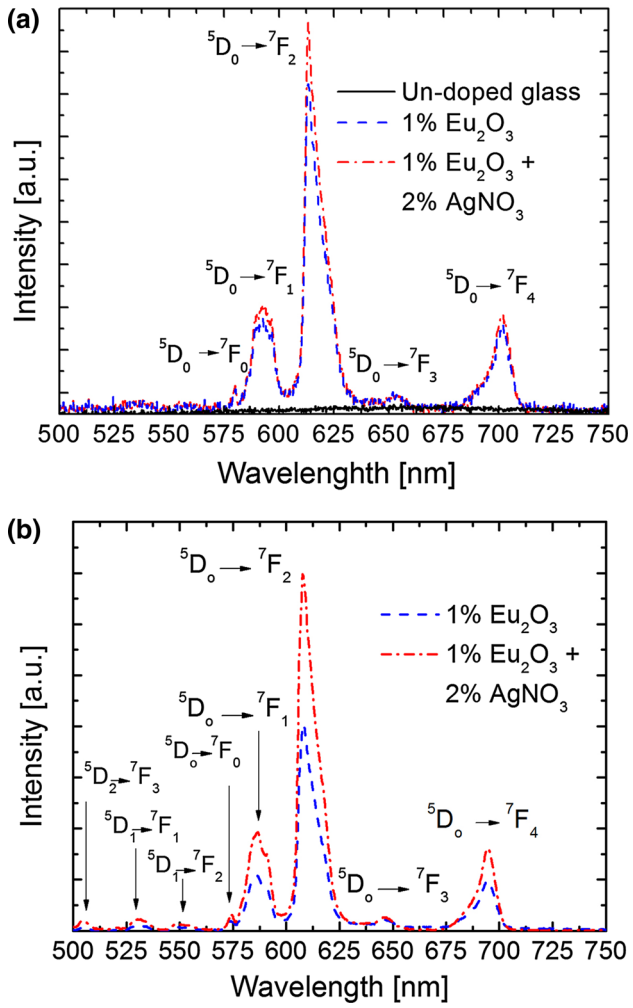


Fig. 3. Emission spectra of $Eu^{3+}$ doped $TeO_2$-ZnO glass samples with and without Ag nanoparticles. Excitation at (a) 405 nm and (b) 473 nm; the un-doped glass is shown as reference.

electric local field around the silver nanoparticles (because of the mismatch between the dielectric function of the metallic nanoparticles and the glass) and also to the energy transfer from the silver nanoparticles to the $Eu^{3+}$ ions,[23–26] whereas for excitation at 405 nm, the enhancement is mainly due to the enhanced local field, because of the detuning of the excitation wavelength with respect to the SPR. On the other hand, quenching of the europium luminescence was reported for high concentrations of metallic nanoparticles and for high concentrations of $Eu_2O_3$.[27,28] Enhancement of the magnetic dipole transition (594 nm) has also been observed.[26] Usually, the magnetic response at optical frequencies is weak; so the location of $Eu^{3+}$ in a region where the electromagnetic field is confined, due to the silver nanoparticles, contributes to the increase of the signal associated with the magnetic dipole transition, and explains the enhancement of the luminescence observed at 594 nm of about 100%. It is similar to the luminescence

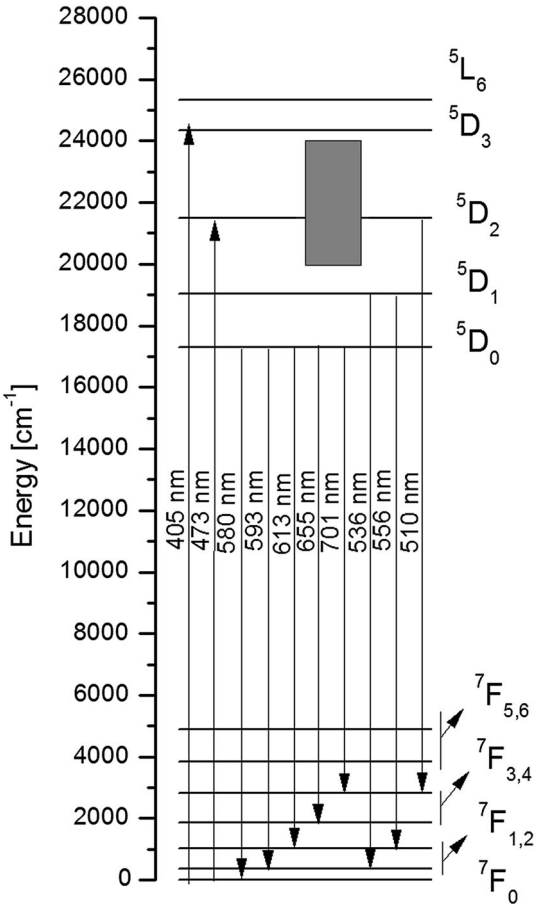


Fig. 4. Simplified energy levels scheme of $Eu^{3+}$ showing the observed transitions under excitation at 405 nm and 473 nm. The shaded area indicates the location of the silver surface plasmon resonance.

enhancement at 614 nm, which in this case is related to an electric dipole transition. In addition, as the magnetic dipole transitions are insensitive to changes in the crystalline fields, we attribute the enhancement of the luminescence at 594 nm to the enhanced optical magnetic field together with the energy transfer from the directly excited nanoparticles.

Electrical characterization of $Eu^{3+}$-doped tellurite glass-covered solar cells are shown in Figs. 5 and 6 for commercial silicon and gallium phosphide solar cells, respectively.

The results have been obtained by comparing the data of the doped and un-doped glass as the cover slip. In this way, we avoid corrections due to reflections. From the $I$–$V$ curves, the short-current circuit ($I_{sc}$), the open-circuit voltage ($V_{oc}$) and the current ($I_{mp}$) and voltage ($V_{mp}$) at the maximum power point were obtained. From these parameters, the efficiency ($\eta$), the fill factor (FF) and the enhancement efficiency (EE) were calculated as:

$$\eta = \frac{V_{mp} I_{mp}}{AI} \tag{1}$$

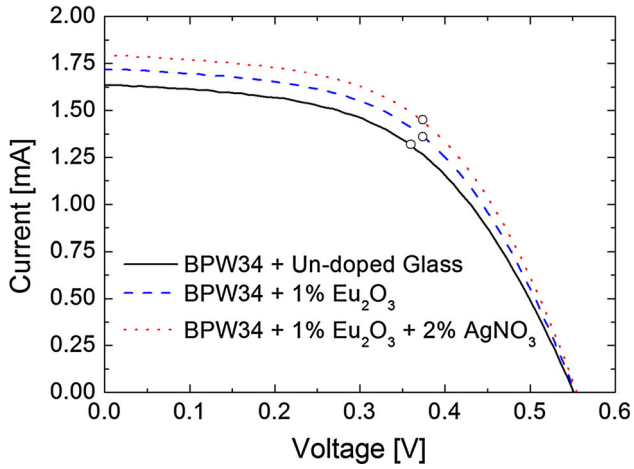


Fig. 5. Electrical characterization of silicon solar cells covered with:un-doped $TeO_2$-ZnO glass, and $Eu_2O_3$-doped $TeO_2$-ZnO glass with and without Ag nanoparticles. Open circles indicate the maximum power point.

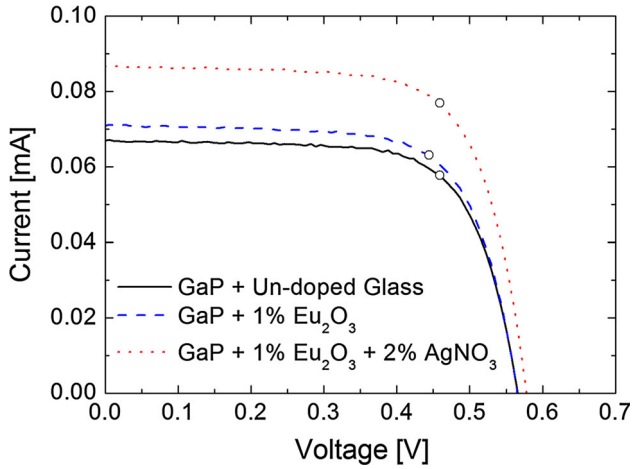


Fig. 6. Electrical characterization of GaP solar cells covered with:un-doped $TeO_2$-ZnO glass, and $Eu_2O_3$-doped $TeO_2$-ZnO glass with and without Ag nanoparticles. Open circles indicate the maximum power points.

$$\mathrm{FF} = \frac{V_{mp} I_{mp}}{V_{oc} I_{sc}} \tag{2}$$

$$\mathrm{EE} = \frac{\eta_{doped} - \eta_{un-doped}}{\eta_{un-doped}} \tag{3}$$

where $A$ is the cell area, $I$ is the incident irradiance (1000 W/m$^2$), and $\eta_{doped}$ and $\eta_{un\text{-}doped}$ are the overall efficiencies of the cell covered with the doped and un-doped glass, respectively. The results are shown in Table I.

For the silicon and GaP solar cells, efficiency enhancements of 7.0% and 5.4% were observed when 1 wt.% of $Eu_2O_3$ was added to the un-doped sample. On the other hand, as the luminescence of the $Eu^{3+}$ ion was increased due to the presence of the silver nanoparticles, in the region with energies

**Table I. Electrical parameters for Si and GaP solar cells covered with $TeO_2$-ZnO glass doped with $Eu^{3+}$, with and without Ag nanoparticles**

| | Matrix doping (%) | | | | | | | | |
|---|---|---|---|---|---|---|---|---|---|
| **Solar cell** | **$Eu_2O_3$** | **$AgNO_3$** | **$I_{sc}$ (mA)** | **$V_{oc}$ (V)** | **$I_{mp}$ (mA)** | **$V_{mp}$ (V)** | **FF** | **$\eta$ (%)** | **EE (%)** |
| BPW34 | 0 | 0 | 1.64 | 0.550 | 1.32 | 0.360 | 0.525 | 5.28 | – |
| | 1 | 0 | 1.72 | 0.550 | 1.36 | 0.374 | 0.537 | 5.65 | 7.0 |
| | 1 | 2 | 1.79 | 0.550 | 1.45 | 0.374 | 0.550 | 6.02 | 14.0 |
| GaP | 0 | 0 | 0.067 | 0.565 | 0.0578 | 0.459 | 0.700 | 0.55 | – |
| | 1 | 0 | 0.071 | 0.565 | 0.0631 | 0.444 | 0.700 | 0.58 | 5.4 |
| | 1 | 2 | 0.087 | 0.572 | 0.0770 | 0.459 | 0.710 | 0.74 | 34.5 |

higher than the energy band gap as shown in Fig. 3, an efficiency enhancement of the solar cell is expected. Efficiency measurements of Si and GaP solar cells covered with glass doped with 1 wt.% of $Eu_2O_3$ and 2 wt.% of $AgNO_3$ revealed enhancements of 14.0% and 34.5% in comparison with the un-doped sample, respectively.

These enhancements can be attributed to the down-conversion mechanisms of the UV radiation and plasmonic effects (energy transfer from the Ag nanoparticles to the $Eu^{3+}$ ions and increase of the local field around the $Eu^{3+}$ ions) or just to the difference of the absorption between the un-doped and doped samples. In order to clarify the contribution of these mechanisms, measurements of the efficiencies were carried out using a modified spectra obtained by filtering the solar spectra with a long-pass colored glass filter ($\lambda > 550$ nm). In this configuration, only the absorption affects the efficiency. The results revealed that the maximum difference between the efficiencies was 0.04%, which represents an enhancement of $10^{-3}$%. This means that the observed efficiency enhancement can be attributed to the down-conversion of UV radiation into visible radiation through the luminescence of the $Eu^{3+}$ ions, as shown in Fig. 3, and not to the difference of the absorption between the un-doped and doped samples.

For comparison, enhancements of about 4.6% have been reported in the literature for silicon solar cells covered with luminescent materials doped with Eu:Dy,[29] and 38% using metal-enhanced nanophosphor fluorescence.[30] Also, it has been reported that Eu/Tb-doped phosphate glass is capable of increasing the photon-to-current efficiency by 3.6 and 6.3%[31] when used to cover amorphous and multicrystalline silicon solar cells, respectively. Luminescent down-shifting layers of CdSe/ZnS quantum dots and Ag nanoparticles in PMMA applied to c-Si and DSSC solar cells showed enhancements of 5.81% and 11.29% in comparison with the sample without Ag nanoparticles, and 1.92% and 3.31% in comparison with the bare cells, respectively. These enhancements were attributed to the absorption and emission of the quantum dots, which were improved with the presence of silver nanoparticles.[32] To our knowledge, the efficiency enhancement values reported here are the highest values obtained in the literature for glass-covered silicon solar cells doped with $Eu^{3+}$ and silver nanoparticles.

## CONCLUSIONS

In conclusion, we have corroborated that the efficiency enhancement of silicon and GaP solar cells covered with tellurite glass can be obtained by the addition of $Eu^{3+}$ ions into the matrix. The measured efficiencies were further improved due to the presence of Ag nanoparticles which enabled an increase of the local field around the $Eu^{3+}$ ion and an energy transfer from the Ag nanoparticles to the $Eu^{3+}$ ions due to the SPR mechanism. These results show the importance of solar spectrum management and the match to the optimal response of the solar cells. The methodology shown here can be applied to other solar cell technologies based on organic and inorganic photovoltaic materials. However, further technological development is required to improve upon these proof-of-concept results.

## ACKNOWLEDGEMENT

The authors acknowledge the Brazilian agencies, Conselho Nacional de Desenvolvimento Científico e Tecnológico (CNPq), Fundacão de Amparo à Ciência e Tecnologia do Estado de Pernambuco (FACEPE) and Escola Politécnica de Pernambuco (POLI–UPE), for financial support. This work was performed under the PRONEX and CNPq (CT Energ 49/2013) Project. We acknowledge the Nanotechnology National Laboratory (LNNano), CNPEM-Campinas/Brazil, for the HR-TEM measurements.

## REFERENCES

1. National Renewable Energy Laboratory (NREL)—National Center for Photovoltaics (NCPV), Research Cell Efficiency Records, (2017). http://www.nrel.gov/ncpv/. Accessed 21 February 2017.
2. M.A. Green, K. Emery, Y. Hishikawa, W. Warta, E.D. Dunlop, D.H. Levi, and A.W.Y. Ho-Baillie, *Prog. Photovolt. Res. Appl.* 25, 3 (2017).
3. H. Lian, Z. Hou, M. Shang, D. Geng, Y. Zhang, and J. Lin, *Energy* 57, 270 (2013).

4. W.J. Ho, G.C. Yang, Y.T. Shen, and Y.J. Deng, *Appl. Surf. Sci.* 365, 120 (2016).
5. J. Wu, J. Wang, J. Lin, Y. Xiao, G. Yue, M. Huang, Z. Lan, Y. Huang, L. Fan, S. Yin, and T. Sato, *Sci. Rep.* 3, 2058 (2013).
6. Z.Q. Li, X.D. Li, Q.Q. Liu, X.H. Chen, Z. Sun, C. Liu, X.J. Ye, and S.M. Huang, *Nanotechnology* 23, 025402 (2012).
7. A.C. Atre, A. García-Etxarri, H. Alaeian, and J.A. Dionne, *J. Opt.* 14, 024008 (2012).
8. S. Derom, A. Berthelot, A. Pillonnet, O. Benamara, A.M. Jurdyc, C. Girard, and G.C. des Francs, *Nanotechnology* 24, 495704 (2013).
9. G. Chen, J. Seo, C. Yang, and P.N. Prasad, *Chem. Soc. Rev.* 42, 8304 (2013).
10. B.S. Richards, *Sol. Energy Mater. Sol. Cells* 90, 2329 (2006).
11. J. Zhou, Y. Teng, S. Ye, G. Lin, and J. Qiu, *Opt. Mater.* 34, 901 (2012).
12. J. Merigeon, O. Maalej, B. Boulard, A. Stanculescu, L. Leontie, D. Mardare, and M. Girtan, *Opt. Mater.* 48, 243 (2015).
13. B. Han, Y. Yang, J. Wu, J. Wei, Z. Li, and Y. Mai, *Ceram. Int.* 41, 12267 (2015).
14. K.R. Catchpole and A. Polman, *Opt. Express* 16, 21793 (2008).
15. M.E. Camilo, E.O. Silva, L.R.P. Kassab, J.A.M. Gracia, and C.B. Araújo, *J. Alloys Compd.* 644, 155 (2015).
16. G.H. Dieke, *Spectra and Energy Levels of Rare Earth Ions in Crystals* (New York: Interscience Publishers, 1968).
17. P.B. Johnson and R.W. Christy, *Phys. Rev. B.* 6, 4370 (1972).
18. V.A.G. Rivera, Y. Ledemi, S.P.A. Osorio, D. Manzani, Y. Messaddeq, L.A.O. Nunes, and E. Marega, *J. Non. Cryst. Solids* 358, 399 (2012).
19. V.P.P. de Campos, L.R.P. Kassab, T.A.A. de Assumpção, D.S. da Silva, and C.B. de Araújo, *J. Appl. Phys.* 112, 063519 (2012).
20. R.J. Amjad, M.R. Dousti, M.R. Sahar, S.F. Shaukat, S.K. Ghoshal, E.S. Sazali, and F. Nawaz, *J. Lumin.* 154, 316 (2014).
21. O.L. Malta and M.A.C. dos Santos, *Chem. Phys. Lett* 174, 13 (1990).
22. M.R. Dousti, *J. Appl. Phys.* 114, 113105 (2013).
23. P.N. Prasad, *Nanophotonics* (Hoboken: Wiley, 2004).
24. R. de Almeida, D.M. da Silva, L.R.P. Kassab, and C.B. de Araújo, *Opt. Commun.* 281, 108 (2008).
25. L.R.P. Kassab, D.S. da Silva, R. de Almeida, and C.B. de Araújo, *Appl. Phys. Lett.* 94, 101912 (2009).
26. L.R.P. Kassab, D.S. da Silva, and C.B. de Araújo, *J. Appl. Phys.* 107, 113506 (2010).
27. T. Hayakawa, S.T. Selvan, and M. Nogami, *J. Non Cryst. Solids* 259, 16 (1999).
28. K. Maheshvaran and K. Marimuthu, *J. Lumin.* 132, 2259 (2012).
29. C. Wang, T. Xuan, J. Liu, H. Li, and Z. Sun, *Int. J. Appl. Ceram. Technol.* 12, 722 (2015).
30. J.Y. Chen, C.K. Huang, W.B. Hung, K.W. Sun, and T.M. Chen, *Sol. Energy Mater. Sol. Cells* 120, 168 (2014).
31. P. Song, C. Zhang, and P. Zhu, *IEEE J. Quantum Electron.* 51, 1 (2015).
32. H. Ahmed, J. Doran, and S.J. McCormack, *Sol. Energy* 126, 146 (2016).